PHYSICS

Polarization-encoded photonic quantum-to-quantum Bernoulli factory based on a quantum dot source

Giovanni Rodari[1], Francesco Hoch[1], Alessia Suprano[1], Taira Giordani[1], Elena Negro[1], Gonzalo Carvacho[1]*, Nicolò Spagnolo[1], Ernesto F. Galvão[2,3], Fabio Sciarrino[1]

A Bernoulli factory is a randomness manipulation routine that takes as input a Bernoulli random variable, outputting another Bernoulli variable whose bias is a function of the input bias. Recently proposed quantum-to-quantum Bernoulli factory schemes encode both input and output variables in qubit amplitudes. This primitive could be used as a subroutine for more complex quantum algorithms involving Bayesian inference and Monte Carlo methods. Here, we report an experimental implementation of a polarization-encoded photonic quantum-to-quantum Bernoulli factory. We present and test three interferometric setups implementing the basic operations of an algebraic field (inversion, multiplication, and addition), which, chained together, allow for the implementation of a generic quantum-to-quantum Bernoulli factory. These in-bulk schemes are validated using a quantum dot–based single-photon source featuring high brightness and indistinguishability, paired with a time-to-spatial demultiplexing setup to prepare input resources of up to three single-photon states.

INTRODUCTION

The so-called Bernoulli Factory (BF) problem was formally introduced by Keane and O'Brien in (*1*), extending a riddle posed by Von Neumann in (*2*) regarding the possibility of obtaining an unbiased coin starting from a biased one. In its classical formulation, the goal of a BF is to construct an algorithm that, starting from independent and identically distributed samples drawn from a Bernoulli variable with unknown bias p, produces as output an exact realization of a Bernoulli variable with bias $f(p)$, for a given well-defined function $f: [0,1] \rightarrow [0,1]$. Since its original formulation, this BF problem has been extended (*3*) and has found application in the development of several fields, such as Monte Carlo methods (*4*, *5*), Bayesian inference (*6*, *7*), and mechanism design (*8*, *9*).

Given the broad applicability of such a problem, in recent years, quantum counterparts to the BF problem were theoretically introduced (*10*–*12*) and experimentally implemented (*13*–*16*). In the quantum-to-classical version of a BF (*10*, *11*), the input classical coin is replaced by a quantum coin represented by a two-dimensional state $|p\rangle$. In this mapping, the state $|p\rangle$ is taken in such a way that if it is measured in the computational basis, it returns a Bernoulli random variable with bias p. It was proven theoretically that with a quantum-to-classical BF, one can implement a strictly larger set of output functions $f(p)$ than its classical counterpart, leading to a quantum advantage in terms of resources needed to perform such a task (*10*, *13*). Stemming from this, the so-called quantum-to-quantum BF (QQBF) concept was introduced (*12*). Here, both the inputs and the outputs of the protocol are quantum resources, and, while it was shown that the set of quantum-to-quantum and classical-to-classical simulable functions have no inclusion relationship with each other (*12*), the formal evaluation of any kind of advantage in terms of resources is, to our knowledge, still an open problem. A direct comparison is made difficult exactly because of the lack of a proper inclusion relation between the classes of functions implementable by quantum and classical Bernoulli factories. Nonetheless, its fully quantum nature makes a QQBF suitable for use as an intermediate step within a broader quantum algorithm. With this in mind, a genuine QQBF implementation should satisfy some requirements. First of all, the QQBF should be oblivious to the input bias p. That is, the scheme used should be able to map—upon suitable post-selection—an arbitrary, unknown state $|p\rangle$ into the state $|f(p)\rangle$. Second, the implementation should feature modularity, i.e., the ability of chaining together several QQBF or integrating them as a processing step in a more general algorithm. Most previous experimental demonstrations of QQBF (*14*, *15*) were essentially unable to fulfill these two requirements.

In this work, we design and implement a genuine QQBF exploiting polarization-encoded photonic qubits and manipulating them within a full in-bulk interferometric setup. With this objective, we exploit a near-deterministic, high-brightness single-photon source (SPS) based on quantum dot (QD) technology, able to generate highly indistinguishable photons. Pairing it with a time-to-spatial demultiplexing setup (DMX), we can prepare the required three-photon states to be injected into a modular implementation of a photonic QQBF with up to two stages, each performing one of the basic operations over a complex field. The paper is organized as follows: We start by describing the main elements required for the construction of a genuine QQBF and our proposed implementation using a photonic polarization–based encoding in a bulk optics setup. We validate the correct operation of the proposed modules by experimentally characterizing the output quantum state fidelity of the two primitive building blocks necessary for the construction of a general QQBF, implementing respectively the (anti-) product and the arithmetic (harmonic) mean functions. Last, we perform a three-photon experiment in which the proposed interferometers are concatenated together in a modular fashion. This allows us to construct a QQBF performing a more complex two-stage function, which can be seen as an instance of a programmable quantum device.

Photonic QQBF

As briefly presented, the QQBF problem is an extension of its classical counterpart (*1*), in which both input and output coins are encoded

[1]Dipartimento di Fisica, Sapienza Università di Roma, P.le Aldo Moro 5, I-00185 Roma, Italy. [2]International Iberian Nanotechnology Laboratory (INL), Av. Mestre José Veiga, 4715-330 Braga, Portugal. [3]Instituto de Física, Universidade Federal Fluminense, Niterói, RJ, Brazil.
*Corresponding author. Email: gonzalo.carvacho@uniroma1.it

in quantum states (Fig. 1, A and B) (*12*). More specifically, given a generic complex number $z \in \mathbb{C}$, we can define the input state as

$$|z\rangle = \frac{z|0_L\rangle + |1_L\rangle}{\sqrt{1+|z|^2}} \quad (1)$$

which is the stereographic projection of the Bloch sphere onto the complex plane. With this mapping, apart from an irrelevant phase factor, a state $|z\rangle$ when measured in the computational basis returns a Bernoulli distribution with bias $p \in \mathbb{R}$ given by:

$$p = \frac{1}{1+|z|^2} \quad (2)$$

The goal of a QQBF is to process a set of quantum coins in the same unknown initial state $|z\rangle$ to return as the final state an output quantum coin in the form:

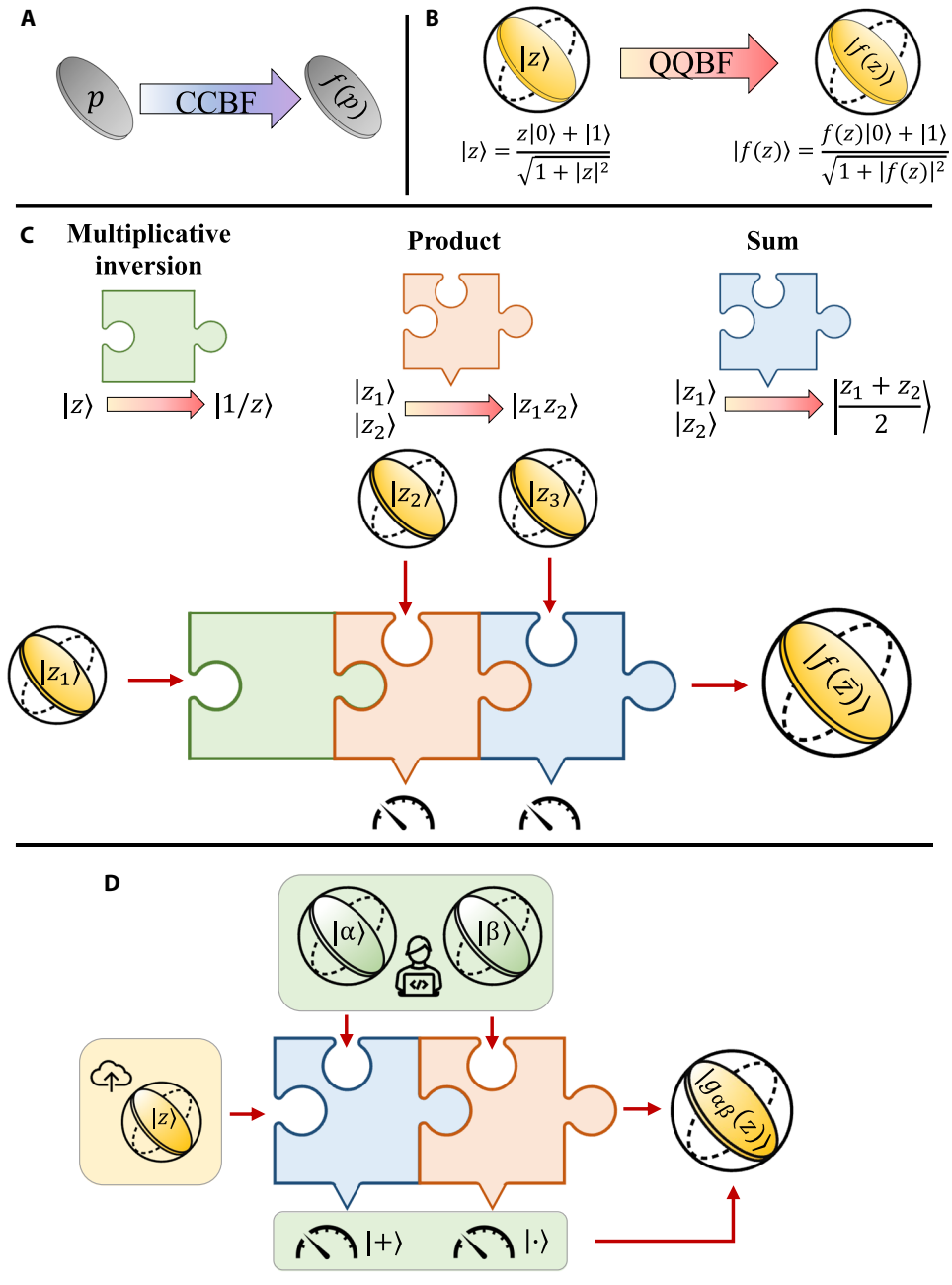

Fig. 1. Main properties of a BF construction. (**A**) Classical-to-classical BF (CCBF). A classical coin with bias p is converted into an output classical coin with bias $f(p)$. (**B**) QQBF. A quantum coin $|z\rangle$ is used as input and manipulated into a quantum state $|f(z)\rangle$. (**C**) Modularity of a QQBF. A QQBF implementing a generic rational function $f(z)$ on the complex field can be obtained by concatenating a set of the three primitive building blocks in a modular fashion: the multiplicative inversion, the product, and the sum. (**D**) Quantum programmability of a QQBF. Given an unknown input quantum coin state, a user can prepare particular quantum states to program the functional shape $g_{\alpha\beta}(z)$ of the transformation to be performed by the QQBF.

$$|f(z)\rangle = \frac{f(z)\,|0_L\rangle + |1_L\rangle}{\sqrt{1+|f(z)|^2}} \tag{3}$$

where $f(z)$ is a chosen function. In (*12*), the necessary and sufficient condition for the existence of a QQBF $|z\rangle \rightarrow |f(z)\rangle$ was found, namely, that the function f belongs to the set of rational functions in the parameter z on the complex field. Note that it can be proven that each function $f(z)$ belonging to the set of rational functions over the complex field can be obtained by simply concatenating the operations of a field, i.e., multiplicative inverse, product, and sum, as depicted in (Fig. 1C). This means that an arbitrary quantum-realizable QQBF can be constructed providing that each primitive field operation can be implemented on its own and concatenated in a modular fashion.

In a photonic formalism fully relying on linear-optical elements (*17*–*19*), practically speaking, the modularity requirement can be enforced in a bias-oblivious way, i.e., with no information on the input state parameters and by encoding both input and output states in a specific photonic degree of freedom, which can be manipulated without affecting the others. We note that in such a modular implementation, a QQBF can also be understood as an instance of a programmable quantum device (*20*–*23*), a paradigm in which a transformation or a measurement performed upon a set of data quantum states is controlled via input program qubits provided by the user. Programmable quantum devices are at the core of delegated blind quantum computing schemes (*24*–*25*). Under this perspective, conceptually depicted in Fig. 1D, the transformation implemented by the QQBF can be chosen and controlled by an external user who provides to the QQBF a set of chosen program quantum registers $\{|\alpha_1\rangle, |\alpha_2\rangle, \ldots\}$. As an example, in this work, we implement a QQBF able to manipulate a single unknown input quantum coin $|z\rangle$ into an output quantum coin $|g_{\alpha_1\alpha_2\ldots}(z)\rangle$, in such a way that the functional form of the bias $g(\cdot)$ is determined by the parameters in the program states. That is, in a three-photon scenario given two program states $|\alpha\rangle$, $|\beta\rangle$, one can implement a QQBF that transforms the bias of unknown input qubit $|z\rangle$ according to any chosen linear function:

$$|z\rangle \otimes |\alpha\rangle\,|\beta\rangle \;\rightarrow\; |\alpha z + \beta\rangle \equiv |g_{\alpha\beta}(z)\rangle \tag{4}$$

A more general description of the space of functions achievable via a genuine implementation of a QQBF protocol is reported in the Supplementary Materials.

In literature, different experiments have attempted to realize a QQBF using photonic-based platforms, but they fail in proposing a general approach in which different operations can be concatenated without any knowledge about the input quantum state (*14*, *15*). We note that recent advances in photonic technologies (*26*) have enabled the realization of system setups comprising several optical spatial modes and components, enabled by the properties and the encoding schemes of integrated platforms (*27*–*30*). However, spatial mode–based encoding schemes may be quite challenging to implement and stabilize for long-distance communication. Therefore, toward a practical integration of a QQBF as a primitive within quantum networks, it is necessary to use a different noise-resilient encoding for long-distance transmission, such as the polarization degree of freedom. While conversion of spatial mode–encoded states to polarization states has been previously achieved on silicon-based on-chip platforms (*31*, *32*), in this context, another approach involves devising protocols that directly use polarization. With this in view, here, we propose an implementation of a genuine QQBF protocol based on in-bulk optical elements, which uses the polarization of distinct photons to encode the input quantum coins $|z\rangle$. In particular, we propose and experimentally characterize the performance of a pair of versatile interferometric setups, which exploit bosonic interference effects among photons to implement the set of primitive field functions $|f(z)\rangle$ required for the construction of a general polarization–based QQBF.

RESULTS

Polarization-based implementation of a QQBF

In this section, we demonstrate how the basic operations of a QQBF—inversion, product, and sum—can be implemented using polarization of single-photon qubits in an in-bulk, photonic linear-optical inteferometric setup. As commonly done in a polarization-based encoding, we identify the horizontal/vertical basis $\{|H\rangle, |V\rangle\}$ of the photon polarization as the computational basis $\{|0_L\rangle, |1_L\rangle\}$. Consequently, the generic state of a quantum coin $|z\rangle$ can be written as:

$$|z\rangle = \frac{z\,|H\rangle + |V\rangle}{\sqrt{1+|z|^2}} \tag{5}$$

With this parameterization, the primitive field operations can be implemented using the interferometers depicted in Fig. 2A, which we now briefly describe.

Multiplicative inversion operation

The inversion operation, defined as $|z\rangle \rightarrow |\frac{1}{z}\rangle$, is performed via a half-wave plate (HWP) with the optical axis placed at an angle of $\pi/4$ radians with respect to the horizontal axis. This is the only operation in the protocol that is deterministic and acts on only one photon.

Product operation

The implementation of the product operation, defined as $|z_1\rangle|z_2\rangle \rightarrow |z_1 z_2\rangle$, requires two photons, with states $|z_1\rangle$ and $|z_2\rangle$, entering into the two input ports of a polarizing beam splitter (PBS). Post-selecting only the events with a single output photon per PBS output mode, we then measure the state of the trigger photon to select the target photon's correct state. Acting on the trigger photon with an HWP having an optical axis rotated by an angle of $\pi/8$ and a PBS, if its polarization is found to be $|V\rangle$ (+ output), the state of the target photon is the product between z_1 and z_2 ($|z_1 z_2\rangle$), while if the polarization is found to be $|H\rangle$ (− output), the target output state is the antiproduct ($|-z_1 z_2\rangle$). In principle, it is possible to always produce the product output $|z_1 z_2\rangle$ by applying a fast polarization rotation, e.g., by means of an electro-optical modulator, acting conditioned upon a detection on the "−" output to recover the correct phase relation. In our implementation, the experiment is performed under post-selection conditions, meaning that the probability of success of the product P_+ and the probability of the antiproduct P_- are given respectively by

$$P_+(z_1, z_2) = P_-(z_1, z_2) = \frac{1+|z_1|^2\,|z_2|^2}{2(1+|z_1|^2)(1+|z_2|^2)} \tag{6}$$

whose maximum $P^{\max}_{+/-} = 0.5$ is attained for input quantum coins satisfying $|z_1|^2 = |z_2|^2 = 0$. Moreover, as discussed in the Supplementary Materials, we have that the success probability becomes null when one has $|z_1\rangle \rightarrow 0$ and $|z_2\rangle \rightarrow |\infty\rangle$, corresponding to a point where the product operation takes an indefinite form.

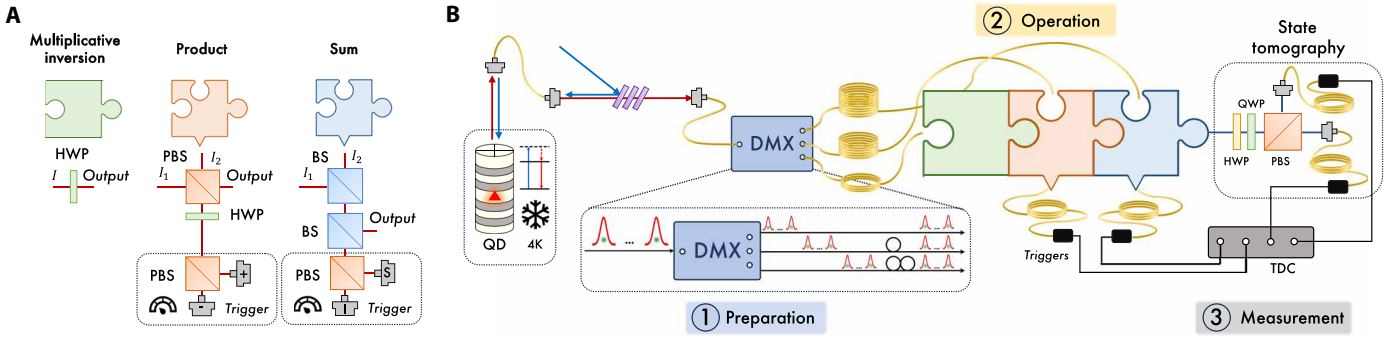

Fig. 2. Polarization-encoded QQBF. (**A**) Primitive building blocks of a polarization-based QQBF: three full in-bulk interferometers implementing the primitive field operations required for a generic QQBF. The input modes of the interferometers are labeled I_1 or I_2. These modules can be concatenated to construct more general functions in a modular approach visualized here as puzzle pieces. (**B**) Full experimental apparatus: We use a QD single-photon source kept in a cryostation at 4 K and operated nonresonantly in the so-called LA phonon–assisted configuration (*38*). The output of the QD source is connected to a time-to-spatial DMX, which distributes the single-photon stream in bunches of ~180 ns toward three output modes: Here, temporal synchronization is achieved via finely tuned in-fiber delay loops. The three-photon resource states are then input to the modular QQBF setup: At its output, the set of projective measurements required for state reconstruction is performed with a sequence of QWPs, HWPs, and PBS. Photon counting events recorded with avalanche photodiodes are processed in a time-to-digital converter where two- or threefold coincidence events with the trigger outputs, denoting that the protocol have succeeded, are suitably post-selected. Legend: PBS, polarizing beam splitter; BS, balanced beam splitter; HWP, half-wave plate; QWP, quarter-wave plate; +/− and S/I, single-photon detectors used, respectively, for product/antiproduct and arithmetic mean/harmonic mean.

Sum operation

To implement the sum operation, defined as $|z_1\rangle|z_2\rangle \Rightarrow |\frac{z_1+z_2}{2}\rangle$, a pair of photons in states $|z_1\rangle$ and $|z_2\rangle$ enter the two input ports of a 50:50 beam splitter (BS). Only the events in which the two photons exit from the same output port are selected. Subsequently, this pair of photons is eventually split in two optical modes through a second BS, and the polarization of the photon exiting the trigger output is measured in the computational basis. If the polarization is found to be $|V\rangle$ (*S* output), then the output state of the target photon is the arithmetic mean ($|\frac{z_1+z_2}{2}\rangle$). Conversely, if the trigger's polarization is found to be $|H\rangle$ (*I* output), the output state is the harmonic mean ($|\frac{2z_1z_2}{z_1+z_2}\rangle$). The exact sum operation $|f(z_1, z_2)\rangle = |z_1 + z_2\rangle$, i.e., without the additional factor two, can be retrieved simply by concatenating with this setup a product block multiplying the output state by this factor. Again, because of the post-selection process, the success probability of the arithmetic mean P_S is given by

$$P_S(z_1, z_2) = \frac{|\frac{z_1+z_2}{2}|^2 + 1}{4(1+|z_1|^2)(1+|z_2|^2)} \tag{7}$$

while the probability of the harmonic mean P_I is expressed as

$$P_I(z_1, z_2) = \frac{|z_1+z_2|^2 + |2z_1z_2|^2}{16(1+|z_1|^2)(1+|z_2|^2)} \tag{8}$$

whose maximum is analytically found to be $P_{S/I}^{\max} = 0.25$. Again, we have some critical points where $P_{S/I}$ becomes null: $(z_1, z_2) = (\infty, \infty)$ for the sum operation and $(z_1, z_2) = (0,0)$ for the harmonic mean operation, as discussed in more detail in the Supplementary Materials.

Concatenation

To devise an optical setup implementing a more complex function, i.e., a generic rational function defined over the complex field, it is essential to be able to concatenate the basic operations. The fact that both input and output photonic qubits are encoded in polarization facilitates this concatenation.

The output from each single building block operation can be used as the input of the next operation, with a clear distinction between post-selected and output modes of each building block. While the success probability will decrease exponentially with the number of building blocks used, it can be proven that any complex operation can be implemented with a finite number of steps. More precisely, to implement a rational function of degree n, the number of required steps is upper bounded by $4n$ (see the Supplementary Materials for a formal demonstration). Furthermore, we remark that finite success probabilities are a feature of general Bernoulli processes and not a limitation that is specific to our proposal.

Experimental verification of the polarization-based QQBF

In this section, we provide a description of the complete experimental apparatus that we used for the verification of the proposed polarization-based modular QQBF scheme. As we briefly summarize in Fig. 2B, the full experimental setup can be divided into three stages: state preparation, operation, and measurement. As described in the figure, we use a QD (*33*–*37*) as a highly efficient, near-deterministic source of single photons. At the output of the QD source, which we operate in the so called nonresonant longitudinal acoustic (LA) phonon-assisted scheme (*33*) at a repetition rate of 79 MHz, we measure a single-photon emission rate of around ~3.5 MHz on avalanche photodiodes. We can assess the quality of the single-photon emission via a standard Hanbury-Brown-Twiss setup, measuring a second-order autocorrelation of around $g^{(2)}(0) \sim 2\%$, while the indistinguishability between subsequently emitted photons evaluated in a Hong-Ou-Mandel interference experiment (*38*) is measured to be $V_{\mathrm{HOM}} \sim 92\%$, as shown in the Supplementary Materials. The output of the QD source is connected via a single-mode fiber to a time-to-spatial DMX, similar to the one described in (*39*, *40*), to distribute the single-photon stream toward three output modes. To achieve up the three-photon resource states used in the present QQBF implementation, time synchronization among photons in the three modes is obtained via in-fiber delay loops of different lengths.

The emission properties of the QD source, characterized by two degenerate energy levels each emitting H/V polarized photons in a

sligthly asymmetric microcavity (*37*), prevent us from achieving a fully polarized single-photon signal at the output of the source. Because of this fact, to achieve full control on the input state preparation, we first select the horizontally polarized component by means of a PBS. Subsequently, we use a pair of HWP and quarter-wave plate (QWP) to encode arbitrary states in the polarization of single photons, as in the mapping given by Eq. 5. After preparing the polarization of the photon states as $|z_i\rangle$, we use them as input in the desired interferometer implementing a primitive QQBF function, as introduced in the previous section. Practically, we note that we had to introduce either an additional HWP or a liquid crystals retarder to compensate for optical phases introduced upon reflection by the mirrors and PBS/BS used in the interferometric setup. As mentioned previously, we post-select only events in which one of the two input photons is collected in the trigger path and the other in the output path. Performing the appropriate measurements on the trigger photon, we ensure that the state of the other photon—the one in the output arm—has been mapped into the desired QQBF result. Upon this post-selection process, in the last stage of the apparatus, we are able to perform quantum state tomography of the output photons' state by means of polarization projections implemented via a QWP, an HWP, and a PBS. Last, to demonstrate the approach's modularity, we concatenate the two setups: The output of the sum block becomes one of the inputs of the product block, while the third photonic resource is taken from the previously unused channel of the DMX. In this setup, exploiting the high intrinsic brightness of the single-photon source paired with the time-to-spatial DMX, data acquisition is carried out on three-photon coincidence events. In this case, the set of three projective measurements (σ_x, σ_y, σ_z) required to perform quantum state tomography and verify that the state of the output photon is the desired one by computing quantum state fidelity must be post-selected upon detection of two photons on a given combination of two trigger outputs.

Validation of the product building block

We first consider the primitive building block implementing the product operation as a QQBF. In our implementation, exploiting the polarization degree of freedom manipulated via in-bulk optical elements, two main noise-inducing effects must be accounted for: (i) the optical phase introduced by reflection through mirrors and the first PBS, which can be corrected by introducing a controlled phase shift between the $|H\rangle$ and $|V\rangle$ polarizations before the heralding measurement; and (ii) the imperfect indistinguishability between the used single photons, i.e., in degrees of freedom different than the polarization, which introduces a degree of impurity in the product/antiproduct density matrix. It can be shown that given a degree of indistinguishability V, the final density matrix of the product/antiproduct operations will respectively be

$$\rho_{\text{prod}} = \frac{1}{1+|z_1 z_2|^2}\begin{pmatrix} |z_1 z_2|^2 & V z_1 z_2 \\ V z_1^* z_2^* & 1 \end{pmatrix} \tag{9}$$

$$\rho_{\text{antiprod}} = \frac{1}{1+|-z_1 z_2|^2}\begin{pmatrix} |-z_1 z_2|^2 & -V z_1 z_2 \\ -V z_1^* z_2^* & 1 \end{pmatrix} \tag{10}$$

as discussed in the Supplementary Materials. To validate the experimental apparatus implementing the product operation, we performed tomography measurements of the states resulting from the product and antiproduct operation between states $|z_1\rangle$ and $|z_2\rangle$ randomly sampled from a uniform distribution of states defined over the Bloch sphere (see Supplementary Materials). We then evaluated the state fidelity (*41*)

$$\mathcal{F} = \text{Tr}\left\{\sqrt{\sqrt{\rho_{\text{exp}}}\sigma_{\text{th}}\sqrt{\rho_{\text{exp}}}}\right\}^2 \tag{11}$$

between the experimentally obtained output state ρ_{exp} and the expected output state $|\sigma_{\text{th}}\rangle$. In Fig. 3, we report the results more than 737 pairs of states, obtaining mean fidelities with the expected output states $|z_1 z_2\rangle$ and $|-z_1 z_2\rangle$ of

$$\begin{aligned} F_{\text{prod}} &= 0.931 \pm 0.040 \\ F_{\text{antiprod}} &= 0.927 \pm 0.043 \end{aligned} \tag{12}$$

These values can be further processed to take into account the imperfect indistinguishability between the used photons. In particular, performing an Hong-Ou-Mandel experiment between the pairs of DMX output photons, we measured a pairwise two-photon visibility of around $V \sim 0.84$. Comparing the obtained experimental data with the expected output density matrices obtained from an ideal operation with input photons having this amount of partial indistinguishability, we find an output average fidelity of

$$\begin{aligned} F^{\text{Exp}}_{\text{prod}} &= 0.983 \pm 0.014, \\ F^{\text{Exp}}_{\text{antiprod}} &= 0.979 \pm 0.019 \end{aligned} \tag{13}$$

Validation of the sum building block

Analogously to what has been discussed for the product operation and also in the sum operation, we have to account for the presence of a polarization-dependent optical phase introduced by reflection on the BSs. Again, this effect can be corrected by placing an HWP in the first preparation arm and a variable phase retarder in the output arm. Similarly to the product operation, we performed a quantum state tomography reconstruction of the states resulting from the arithmetic and harmonic mean operations between state pairs $|z_1\rangle$ and $|z_2\rangle$ randomly sampled from a uniform distribution of states defined over the Bloch sphere (see the Supplementary Materials). We report in Fig. 3 the results more than 1007 pairs of states, obtaining average fidelities with the expected states $|\frac{z_1+z_2}{2}\rangle$ and $|\frac{2z_1 z_2}{z_1+z_2}\rangle$ of

$$\begin{aligned} F_{\text{sum}} &= 0.934 \pm 0.070 \\ F_{\text{amean}} &= 0.946 \pm 0.057 \end{aligned} \tag{14}$$

respectively. Again, this result can be further processed to take into account the imperfect indistinguishability V in the expected output state, where the formal dependence of the output density matrices with V is reported in the Supplementary Materials. By considering a two-photon visibility of around $V \sim 0.84$, we obtain the following average fidelities

$$\begin{aligned} F^{\text{Exp}}_{\text{sum}} &= 0.973 \pm 0.025, \\ F^{\text{Exp}}_{\text{amean}} &= 0.978 \pm 0.022. \end{aligned} \tag{15}$$

We note that when considering the fidelities of the experimentally obtained states with respect to the theoretical model assuming perfect indistinguishability, for around 3% of the output states, we obtain values lower than 0.75: This is due to the fact that, with the used

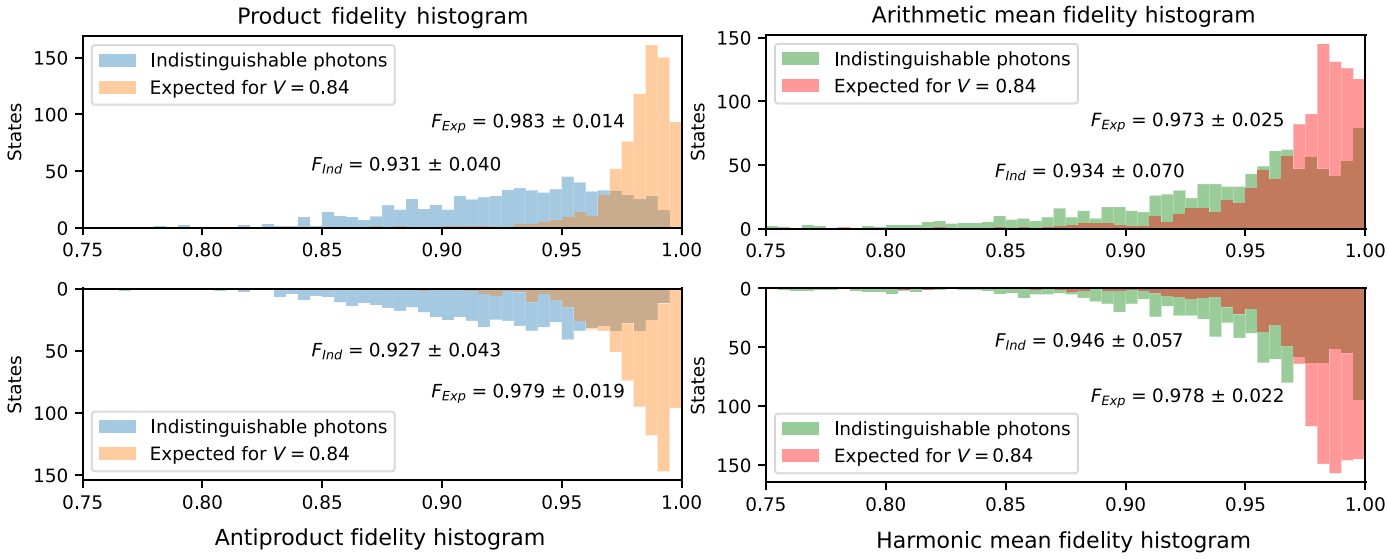

Fig. 3. Fidelity of the output states from the basic operation interferometers. On the left side, histograms of the fidelity for product and antiproduct operation evaluated more than 737 random pairs of states $|z_1\rangle$ and $|z_2\rangle$ uniformly drawn from the Bloch sphere. On the right, histograms of the fidelity for the arithmetic and harmonic mean operation evaluated ,more than 1007 random pairs of states $|z_1\rangle$ and $|z_2\rangle$ uniformly drawn from the Bloch sphere. The fidelities are shown both with respect to the ideal output pure state $|f(z)\rangle$ and with respect to the state expected when taking into account the estimated imperfect photonic indistinguishability.

scheme, the corresponding input pairs $\{|z_1\rangle, |z_2\rangle\}$ appear to be more sensitive to both an imperfect compensation of the polarization-dependent phase shift introduced by the first BS and imperfect indistinguishability. When accounting for the latter effect, the corrected visibility for such states lies in all cases in the interval (0.75,0.9), i.e., the tail of the overall distribution reported in Fig. 3. Considering both the sum-block and the product-block, we obtain a high average fidelity with respect to randomly chosen input pairs $\{z_1, z_2\}$. We obtain an average fidelity with respect to the expected pure output states of $\overline{F} = (0.933 \pm 0.024)$, certifying the correct behavior of the overall implementation of the QQBF building blocks without accounting for sources of experimental noise of the present implementation, i.e., nonideal optical elements and imperfect photonic indistinguishability. Accounting for the latter effect in terms of a correction applied to the expected output density matrices, we obtain an average fidelity of $\overline{F}_{\mathrm{Exp}} = (0.978 \pm 0.020)$, which is a benchmark of how we could expect the proposed optical setups to perform with the use of ideal photonic resources.

Polarization-based QQBF as a modular programmable setup

As the natural next step, we then experimentally tested whether the implemented in-bulk interferometers, discussed in the previous sections, could be chained together in a modular fashion via redirecting the output of a given block to the input of the subsequent one, an essential requirement toward the implementation of a photonic-based QQBF implementing a generic function $|f(z)\rangle$. By chaining together the sum and product modules depicted in Fig. 2A, one obtains a QQBF implementing, upon post-selection on the corresponding pair of trigger outputs, one of four possible functions $|f(z_1, z_2, z_3)\rangle$ among the three unknown input quantum coins $\{|z_1\rangle, |z_2\rangle, |z_3\rangle\}$: sum-product, harmonic mean-product, sum-antiproduct, and harmonic mean-antiproduct. From another perspective, we note that such a scenario, featuring two concatenated modules and three input photons, can be interpreted as the photonic realization of a programmable setup implementing the linear transformation of Eq. 4. As a specific example, we identify the state $|z_1\rangle$ of one input photon as the data state $|z\rangle$ and treating the other two inputs $\{|z_2\rangle, |z_3\rangle\}$ as program states provided by the user. One can then realize both linear transformations given by

$$|z\rangle \otimes |\alpha\rangle |\beta\rangle \rightarrow |\pm\alpha z \pm \beta\rangle \tag{16}$$

In our implementation, these functions are realized by choosing

$$|z_1\rangle = |z\rangle; \quad |z_2\rangle = \left|\frac{\beta}{\alpha}\right\rangle; \quad |z_3\rangle = |2\alpha\rangle \tag{17}$$

since it can be easily shown that after the linear optical transformation obtained by chaining together the sum and product modules, the overall output state will be either in the state

$$\left|\frac{z+\beta/\alpha}{2}\cdot(2\alpha)\right\rangle = |\alpha z + \beta\rangle \tag{18}$$

or in the state

$$\left|-\frac{z+\beta/\alpha}{2}\cdot(2\alpha)\right\rangle = |-\alpha z - \beta\rangle \tag{19}$$

upon the post-selection process conditioned on the detection of one photon in the state $|S\rangle$ at the sum trigger output together with a photon at the product trigger output respectively in state $|+\rangle$ or in state $|-\rangle$.

To experimentally test the feasibility of this approach, we realized the interconnection between the two optical interferometers via a single-mode fiber, linking the sum output port to the input I_1 of the product interferometer in Fig. 2A. To compensate both for unwanted phases introduced by reflections in the product and sum setup, as well as the unchanged polarization state at the output of

the sum setup, we introduce a set of paddles to compensate for the unknown unitary induced by the single-mode fiber on the polarization space. Encoding different polarization states $|z_1\rangle$, $|z_2\rangle$ as input of the sum setup and $|z_3\rangle$ as the free input in the product setup, we first evaluated the outcome of each of the four possible function combinations: sum-product, harmonic mean-product, sum-antiproduct, and harmonic mean-antiproduct. The crucial use of a QD-based bright SPS paired with a highly efficient time-to-spatial DMX enabled us to experimentally perform a threefold quantum state tomography for each combination. In particular, we considered 30 different sets $\{|z_1\rangle, |z_2\rangle, |z_3\rangle\}$ of input states, and for each of these, we computed the fidelity associated with the four expected ideal output states, represented as black outlined bars in Fig. 4A. As briefly discussed in the previous sections and also in this scenario, it is necessary to account for the noise introduced by the finite degree of indistinguishability. As indicated by the shaded bars in Fig. 4A, the output state fidelity—our figure of merit for the experiment—generally improves when we consider the expected output states corrected for the limited degree of indistinguishability among the interfering single-photon states—assumed to be approximately $V \sim 0.84$, as reported in the Supplementary Materials. Note that there are triples of inputs $\{|z_1\rangle, |z_2\rangle, |z_3\rangle\}$ for which the resulting density matrices do not depend on the visibility V, thus resulting in an output fidelity that is unaffected by this correction. Empty regions at the center of each bar plot indicate input choices for which the resulting function succeeds with null probability. In Table 1, we report the average fidelities, computed more than the 30 input sets $\{|z_1\rangle, |z_2\rangle, |z_3\rangle\}$, with respect to each possible combination obtainable by cascading together the sum and the product-building blocks. The average overall fidelity accounting for the visibility correction is found to be

$$\overline{F}^{\mathrm{Exp}}_{3-\mathrm{fold}} = 0.931 \pm 0.017 \tag{20}$$

which shows that the proposed polarization-based encoding and the fully in-bulk experimental schemes can be indeed chained together in a fashion that is both modular and oblivious about the input biases $\{|z_1\rangle, |z_2\rangle, |z_3\rangle\}$, two essential requirements for the implementation of a genuine version of a photonic QQBF.

As briefly discussed at the beginning of this section, we can interpret the photonic concatenation of two QQBF primitive modules as an instance of a device implementing the family of linear functions $|\pm g_{\alpha\beta}(z)\rangle = |\pm\, \alpha z \pm \beta\rangle$. This perspective has one of the input photons interpreted as a data qubit $|z\rangle$, possibly unknown to the experimenter and provided by an external user, while the other two can be fixed by the experimenter to be $|\beta/\alpha\rangle$ and $|2\alpha\rangle$ so as to choose the parameters of the implemented function $g_{\alpha\beta}$ in a programmable fashion. In Fig. 4B, we focus on the results obtained for the QQBF implementing the function $|g_{\alpha\beta}(z)\rangle = |\alpha z + \beta\rangle$, recovered when post-selecting upon the detection of a photon in the *S*-output of the sum module and on the $|+\rangle$-output of the product module. In particular, we report the experimentally obtained fidelities with respect to the (non) corrected output states for three different choices of programmable parameters (α, β), corresponding to ($\alpha = \beta = 1/2$), ($\alpha = 1/2, \beta = 0$), and ($\alpha = -\,i/2, \beta = 0$). A comparison between the experimentally obtained density matrices and the expected ones is

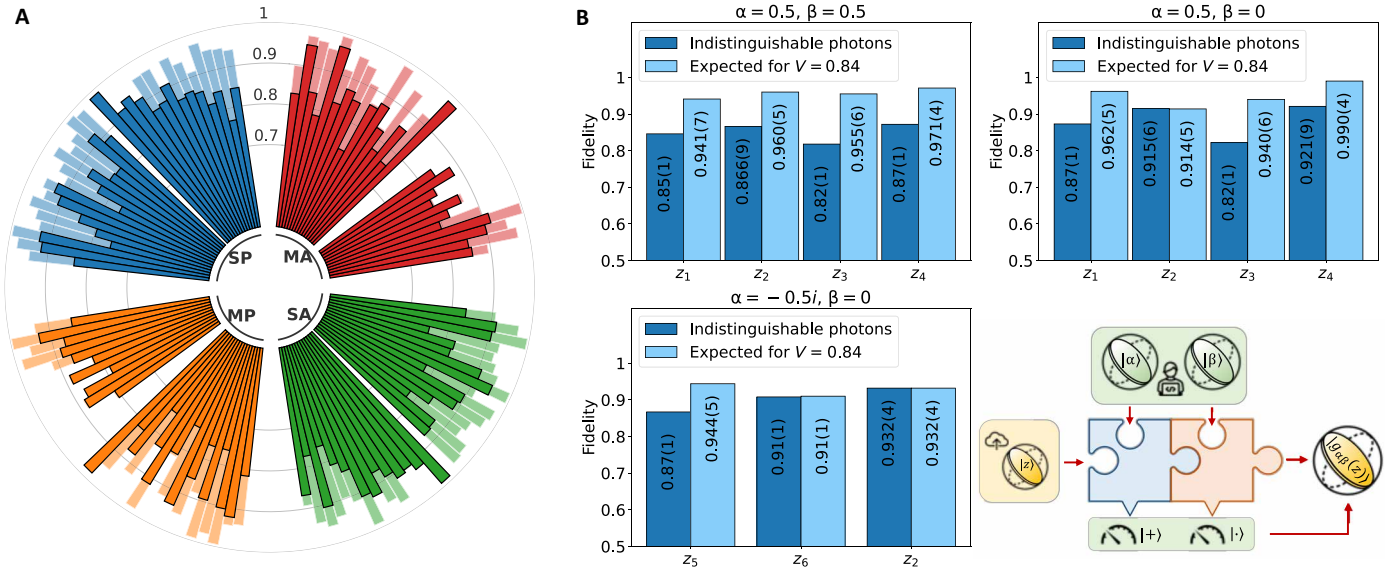

Fig. 4. Performance of the concatenated QQBF primitive modules as a programmable device. (**A**) Circular bar plot of the output quantum state fidelities, comparing the theoretical state with the one reconstructed via quantum state tomography, for each possible combination of concatenated operations. The black outlined bars represent the fidelities obtained with respect to the theoretically predicted pure output state; on top, the shaded bars represent the fidelity with respect to the state corrected for imperfect photonic indistinguishability. The absence of a bar corresponds to a null post-selection probability. (**B**) Interpretation of the results obtained by concatenating the sum and product primitive building blocks to implement a programmable QQBF producing the family of linear transformations $|\pm g_{\alpha\beta}(z)\rangle = |\pm\alpha \pm \beta z\rangle$. The three-bar plots depict the experimentally obtained fidelities when computing the output function $|g_{\alpha\beta}(z)\rangle = |\alpha z + \beta\rangle$ for different choices of the input data states *z*, namely $\{z_1, z_2, z_3, z_4, z_5, z_6\} = \{1{,}0, -0.27 - i0.74, -0.27 + i0.74, -i, \infty\}$, and pairs of parameters (α, β). The program states at the input of the sum module and the product module, respectively, were chosen as $|\beta/\alpha\rangle$ and $|2\alpha\rangle$, so the pair of programming parameters are (α, β) = {(1/2,1/2), (1/2,0), (−*i*/2,0)} in the function $g_{\alpha\beta}(z)$. The darker and lighter blue bars show the quantum state fidelity between the experimentally reconstructed state and, respectively, the output state corresponding to completely indistinguishable input photons, and the state expected from an ideal operation with the experimentally characterized imperfect photonic indistinguishability.

Table 1. Threefold fidelity. Average fidelities computed more than 30 input triplets $\{|z_1\rangle, |z_2\rangle, |z_3\rangle\}$ for each of the four operation combinations (sum-product, harmonic mean-product, sum-antiproduct, and harmonic mean-antiproduct). The reported values refer to the ideal case in which perfect indistinguishability is considered ($V = 1$) and to the experimental indistinguishability scenario ($V = 0.84$). The first two table columns also represent the average fidelities for the photonic QQBF interpreted as a programmable setup, implementing the transformation $|\pm g_{\alpha\beta}(z)\rangle = |\pm\alpha z \pm \beta\rangle$.

V	F_{SP}	F_{MP}	F_{SA}	F_{MA}
1	0.865 ± 0.055	0.851 ± 0.061	0.866 ± 0.059	0.849 ± 0.058
0.84	0.951 ± 0.024	0.916 ± 0.061	0.945 ± 0.030	0.913 ± 0.059

provided in the Supplementary Materials. Furthermore, by considering all the 30 chosen input triplets, we obtain an overall average corrected fidelity of $\widehat{F}_{\alpha z+\beta} = 0.951 \pm 0.024$ and $\widehat{F}_{-\alpha z-\beta} = 0.945 \pm 0.030$, showing that with our proposed polarization-encoded photonic setups, we can provide a proof-of-principle realization of a programmable QQBF implementing the linear transformations $|\pm g_{\alpha\beta}(z)\rangle = |\pm\alpha z \pm \beta\rangle$.

DISCUSSION

In this work, we devised and experimentally verified a solution to the quantum counterpart of the so-called BF problem, i.e., a randomness manipulation protocol which generates, starting from quantum coins in a state $|z\rangle \propto z|0\rangle + |1\rangle$, an output state $|f(z)\rangle$ where $f(z)$ is a rational function defined on the complex field. In the present scheme, the primitive field functions from which arbitrary QQBF can be constructed have been implemented by using two fully in-bulk interferometric schemes, in which the required operations are realized as probabilistic gates acting on polarization-encoded photonic qubits. In particular, we experimentally tested the performance of the proposed interferometric setups both in the single-operation scenario and when two modules are concatenated, verifying not only the obliviousness of our schemes to the input state bias but also the modularity of our approach, both requirements for a genuine implementation of a QQBF. Moreover, we show how a QQBF where two or more modules are cascaded together can be interpreted as a programmable platform to perform an operation $g_{\alpha 1\alpha 2\ldots}(z)$ on an unknown input state $|z\rangle$, parameterized by a set of auxiliary program states $|\alpha_1, \alpha_2, \ldots\rangle$, and presented an implementation of the function $|\alpha z + \beta\rangle$ as an example. Our QQBF is implemented in a state-of-the-art hybrid photonic platform, composed of a high-brightness SPS based on the QD technology interfaced with an active time-to-spatial DMX, tailored for the efficient generation of multiphoton resource states. This enables us to validate the present polarization-based photonic QQBF implementation via a reconstruction of the output state even in the more complex three-photon scenario. Moreover, even if the proposed scheme relies on bosonic interference effects and measurement post-selection thus being intrinsically probabilistic, one could take advantage of the near-deterministic properties of the QD emission to increase the final success probability of the protocol via the addition of a feedback-controlled active modulation system. This approach would provide an essential element toward the scalability of the proposed modular implementation of QQBF to perform complex functions requiring a higher number of modules chained together since the implementation of n modules requires $n + 1$ single-photon states. Given its probabilistic nature, a thorough analysis of the resource overhead of the protocol would be of interest to assess a practical application of our protocol and is left as future work. Recent technological advances have shown the capability of moving photonic experiments toward regimes with larger photon numbers (*30*, *42*, *43*). Hence, given the maturity of photonic quantum technologies and considering that polarization encoded photonic qubits are a naturally suitable and resilient resource when transmitted over long distances, our results could pave the way toward the use of a QQBF, or similar randomness manipulation schemes, as a subroutine in a distributed computation over a complex quantum network.

MATERIALS AND METHODS

Our QD emitter is a single self-assembled InGaAs QD embedded at the center of an electrically controlled microcavity surrounded by two Braggs reflectors made of GaAs/Al $_{0.95}$Ga $_{0.05}$As $\lambda/4$ layers with 36 (16) pairs for the bottom (top) (*36*) to enhance the spontaneous emission via Purcell effect and enabling collection in a single-mode fiber atop of the source. We use a nonresonant emission geometry known as LA phonon-assisted configuration (*33*): upon being excited with a 79-MHz–pulsed laser source at a wavelength of 927.2 nm, photons are emitted nonresonantly at a wavelength of 927.8 ± 0.2 nm and separated from the residual pump laser through a sequence of three narrow band-pass filters. The QD source is housed on a commercially available solution—Quandela e-Delight chip—and the SPS is kept at 4 K in a low-vibration closed-cycle He cryostat Attocube Attodry 800. Pulse shaping of the 79-MHz–pulsed pump laser is obtained through a commercial 4f to select the required excitation central wavelength of 927.2 nm and achieve an ~100-pm spectral bandwidth. As stated in the section "Experimental verification of the polarization-based QQBF", the typical count rate at the output of the SPS is around 3.5 MHz when measured with avalanche photodiodes featuring a quantum efficiency of ~35%, corresponding to a first-lens brightness of ~24%. The stream of single photons emitted by the QD is then sent to the time-to-spatial DMX. Here, we have an optical setup that, by means of the spatial diffraction induced by an acousto-optical modulator, divides the input signal in bunches of ~180 ns sequentially and periodically redirected toward three output channels, akin to the scheme used in (*29*, *40*). As stated in the main text, the signals from these outputs are collected in single-mode fibers, which are delay loops of different lengths, to temporally synchronize the photon bunches exiting each of the three output channels, rendering them temporally indistinguishable.

Supplementary Materials

This PDF file includes:

Supplementary Text
Figs. S1 to S3
Table S1

REFERENCES AND NOTES

1. M. Keane, G. L. O'Brien, A Bernoulli factory. *ACM Trans. Model. Comp. Simul.* **4**, 213–219 (1994).
2. V. Neumann, Various techniques used in connection with random digits. *Appl. Math Ser.* **12**, 36 (1951).
3. R. P. Lem, J. Schneider, Multiparameter Bernoulli factories. arXiv:2202.07216 [math.PR] (2022).
4. J. M. Flegal, R. Herbei, Exact sampling for intractable probability distributions via a Bernoulli factory. *Electron. J. Stat.* **6**, 10–37 (2012).
5. D. Vats, F. B. Gonçalves, K. Łatuszyński, G. O. Roberts, Efficient Bernoulli factory markov chain Monte Carlo for intractable posteriors. *Biometrika* **109**, 369–385 (2022).
6. F. B. Goncalves, K. Łatuszynski, G. O. Roberts, Exact Monte Carlo likelihood-based inference for jump-diffusion processes. *Stat. Methodol.* **85**, 732–756 (2023).
7. R. Herbei, L. M. Berliner, Estimating ocean circulation: An MCMC approach with approximated likelihoods via the Bernoulli factory. *J. Am. Stat. Assoc.* **109**, 944–954 (2014).
8. S. Dughmi, J. Hartline, R. D. Kleinberg, R. Niazadeh, Bernoulli factories and black-box reductions in mechanism design. *J. ACM* **68**, 1–30 (2021).
9. Y. Cai, A. Oikonomou, G. Velegkas, M. Zhao, An Efficient ε-BIC to BIC Transformation and Its Application to Black-Box Reduction in Revenue Maximization, in *Proceedings of the 2021 ACM-SIAM Symposium on Discrete Algorithms (SODA)* (Society for Industrial and Applied Mathematics, 2021) pp. 1337–1356.
10. H. Dale, D. Jennings, T. Rudolph, Provable quantum advantage in randomness processing. *Nat. Commun.* **6**, 8203 (2015).
11. H. Dale, "Quantum coins and quantum sampling," thesis, Imperial College London, London, UK. (2016).
12. J. Jiang, J. Zhang, X. Sun, Quantum-to-quantum bernoulli factory problem. *Phys. Rev. A* **97**, 032303 (2018).
13. R. B. Patel, T. Rudolph, G. J. Pryde, An experimental quantum Bernoulli factory. *Sci. Adv.* **5**, eaau6668 (2019).
14. X. Zhan, K. Wang, L. Xiao, Z. Bian, P. Xue, Experimental demonstration of quantum-to-quantum Bernoulli factory. *Phys. Rev. A* **102**, 012605 (2020).
15. Y. Liu, J. Jiang, P. Zhu, D. Wang, J. Ding, X. Qiang, A. Huang, P. Xu, J. Zhang, G. Tian, X. Fu, M. Deng, C. Wu, X. Sun, X. Yang, J. We, General quantum Bernoulli factory: Framework analysis and experiments. *Quant. Sci. Technol.* **6**, 045025 (2021).
16. X. Yuan, K. Liu, Y. Xu, W. Wang, Y. Ma, F. Zhang, Z. Yan, R. Vijay, L. Sun, X. Ma, Experimental quantum randomness processing using superconducting qubits. *Phys. Rev. Lett.* **117**, 010502 (2016).
17. P. Kok, W. J. Munro, K. Nemoto, T. C. Ralph, J. P. Dowling, G. J. Milburn, Linear optical quantum computing with photonic qubits. *Rev. Mod. Phys.* **79**, 135–174 (2007).
18. S. Slussarenko, G. J. Pryde, Photonic quantum information processing: A concise review. *Appl. Phys. Rev.* **6**, 041303 (2019).
19. F. Flamini, N. Spagnolo, F. Sciarrino, Photonic quantum information processing: A review. *Rep. Prog. Phys.* **82**, 016001 (2018).
20. M. A. Nielsen, I. L. Chuang, Programmable quantum gate arrays. *Phys. Rev. Lett.* **79**, 321–324 (1997).
21. M. Dušek, V. Bužek, Quantum-controlled measurement device for quantum-state discrimination. *Phys. Rev. A* **66**, 022112 (2002).
22. M. Roško, V. Bužek, P. R. Chouha, M. Hillery, Generalized measurements via a programmable quantum processor. *Phys. Rev. A* **68**, 062302 (2003).
23. M. Ziman, V. Buzek, Realization of positive-operator-valued measures using measurement-assisted programmable quantum processors. *Phys. Rev. A* **72**, 022343 (2005).
24. J. F. Fitzsimons, E. Kashefi, Unconditionally verifiable blind quantum computation. *Phys. Rev. A* **96**, 012303 (2017).
25. B. Polacchi, D. Leichtle, L. Limongi, G. Carvacho, G. Milani, N. Spagnolo, M. Kaplan, F. Sciarrino, E. Kashefi, Multiclient distributed blind quantum computation with the qline architecture. *Nat. Commun.* **14**, 7743 (2023).
26. J. Wang, F. Sciarrino, A. Laing, M. G. Thompson, Integrated photonic quantum technologies. *Nat. Photonics* **14**, 273–284 (2020).
27. F. Flamini, L. Magrini, A. S. Rab, N. Spagnolo, V. D'Ambrosio, P. Mataloni, F. Sciarrino, T. Zandrini, A. Crespi, R. Ramponi, R. Osellame, Thermally reconfigurable quantum photonic circuits at telecom wavelength by femtosecond laser micromachining. *Light Sci. Appl.* **4**, e354 (2015).
28. W. R. Clements, P. C. Humphreys, B. J. Metcalf, W. S. Kolthammer, I. A. Walmsley, Optimal design for universal multiport interferometers. *Optica* **3**, 1460 (2016).
29. C. Taballione, R. van der Meer, H. J. Snijders, P. Hooijschuur, J. P. Epping, M. de Goede, B. Kassenberg, P. Venderbosch, C. Toebes, H. van den Vlekkert, P. W. H. Pinkse, J. J. Renema, A universal fully reconfigurable 12-mode quantum photonic processor. *Mater. Quant. Technol.* **1**, 035002 (2021).
30. N. Maring, A. Fyrillas, M. Pont, E. Ivanov, P. Stepanov, N. Margaria, W. Hease, A. Pishchagin, T. H. Au, S. Boissier, E. Bertasi, A. Baert, M. Valdivia, M. Billard, O. Acar, A. Brieussel, R. Mezher, S. C. Wein, A. Salavrakos, P. Sinnott, D. A. Fioretto, P.-E. Emeriau, N. Belabas, S. Mansfield, P. Senellart, J. Senellart, N. Somaschi, A versatile single-photon-based quantum computing platform. *Nat. Photonics* **18**, 603–609 (2024).
31. C. Ma, W. D. Sacher, Z. Tang, J. C. Mikkelsen, Y. Yang, F. Xu, T. Thiessen, H.-K. Lo, J. K. Poon, Silicon photonic transmitter for polarization-encoded quantum key distribution. *Optica* **3**, 1274 (2016).
32. D. Llewellyn, Y. Ding, I. I. Faruque, S. Paesani, D. Bacco, R. Santagati, Y.-J. Qian, Y. Li, Y.-F. Xiao, M. Huber, M. Malik, G. F. Sinclair, X. Zhou, K. Rottwitt, J. L. O'Brien, J. G. Rarity, Q. Gong, L. K. Oxenlowe, J. Wang, M. G. Thompson, Chip-to-chip quantum teleportation and multi-photon entanglement in silicon. *Nat. Phys.* **16**, 148–153 (2020).
33. S. Thomas, M. Billard, N. Coste, S. Wein, H. Ollivier, O. Krebs, L. Tazaırt, A. Harouri, A. Lemaitre, I. Sagnes, C. Anton, L. Lanco, N. Somaschi, J. C. Loredo, P. Senellart, Bright polarized single-photon source based on a linear dipole. *Phys. Rev. Lett.* **126**, 233601 (2021).
34. O. Gazzano, S. Michaelis de Vasconcellos, C. Arnold, A. Nowak, E. Galopin, I. Sagnes, L. Lanco, A. Lemaˆıtre, P. Senellart, Bright solid-state sources of indistinguishable single photons. *Nat. Commun.* **4**, 1425 (2013).
35. A. Nowak, S. Portalupi, V. Giesz, O. Gazzano, C. Dal Savio, P.-F. Braun, K. Karrai, C. Arnold, L. Lanco, I. Sagnes, A. Lemaitre, P. Senellart, Deterministic and electrically tunable bright single-photon source. *Nat. Commun.* **5**, 3240 (2014).
36. N. Somaschi, V. Giesz, L. De Santis, J. Loredo, M. P. Almeida, G. Hornecker, S. L. Portalupi, T. Grange, C. Anton, J. Demory, C. Gomez, I. Sagnes, N. D. Lanzillotti-Kimura, A. Lemaitre, A. Auffeves, A. G. White, L. Lanco, P. Senellart, Nearoptimal single-photon sources in the solid state. *Nat. Photonics* **10**, 340–345 (2016).
37. H. Ollivier, I. M. de Buy Wenniger, S. Thomas, S. C. Wein, A. Harouri, G. Coppola, P. Hilaire, C. Millet, A. Lemaitre, I. Sagnes, O. Krebs, L. Lanco, J. C. Loredo, C. Anton, N. Somaschi, P. Senellart, Reproducibility of high-performance quantum dot single-photon sources. *ACS Photonics* **7**, 1050–1059 (2020).
38. C.-K. Hong, Z.-Y. Ou, L. Mandel, Measurement of subpicosecond time intervals between two photons by interference. *Phys. Rev. Lett.* **59**, 2044–2046 (1987).
39. M. Pont, G. Corrielli, A. Fyrillas, I. Agresti, G. Carvacho, N. Maring, P.-E. Emeriau, F. Ceccarelli, R. Albiero, P. H. D. Ferreira, N. Somaschi, J. Senellart, I. Sagnes, M. Morassi, A. Lemaitre, P. Senellart, F. Sciarrino, M. Liscidini, N. Belabas, R. Osellame, High-fidelity four-photon GHZ states on chip. *npj Quan. Inf.* **10**, 50 (2024).
40. M. Pont, R. Albiero, S. E. Thomas, N. Spagnolo, F. Ceccarelli, G. Corrielli, A. Brieussel, N. Somaschi, H. Huet, A. Harouri, A. Lemaitre, I. Sagnes, N. Belabas, F. Sciarrino, R. Osellame, P. Senellart, A. Crespi, Quantifying n-photon indistinguishability with a cyclic integrated interferometer. *Phys. Rev. X* **12**, 031033 (2022).
41. R. Jozsa, Fidelity for mixed quantum states. *J. Mod. Opt.* **41**, 2315–2323 (1994).
42. H. Cao, L. Hansen, F. Giorgino, L. Carosini, P. Zahalka, F. Zilk, J. Loredo, P. Walther, Photonic source of heralded Greenberger-Horne-Zeilinger states. *Phys. Rev. Lett.* **132**, 130604 (2024).
43. L. M. Hansen, L. Carosini, L. Jehle, F. Giorgino, R. Houvenaghel, M. Vyvlecka, J. C. Loredo, P. Walther, Single-active-element demultiplexed multi-photon source. *Optica Quant.* **1**, 1–5 (2023).

Acknowledgments

Funding: This work was supported by the ERC Advanced Grant QU-BOSS (QUantum advantage via nonlinear BOSon Sampling, grant agreement no. 884676) and by ICSC–Centro Nazionale di Ricerca in High Performance Computing, Big Data and Quantum Computing, funded by European Union–NextGenerationEU. E.F.G. acknowledges support from FCT - Fundação para a Ciência e a Tecnologia (Portugal) via project CEECINST/00062/2018. **Author contributions:** F.H., T.G., G.C., N.S., E.F.G., and F.S. conceived the scheme for the polarization-encoded Quantum-to-Quantum Bernoulli Factory. G.R., F.H., A.S., T.G., G.C., N.S., and F.S. conceived the experimental platform. G.R., F.H., A.S., T.G., E.N., G.C., N.S., and F.S. performed the experiment and carried out the data analysis. All authors contributed to discussing the results and to writing the manuscript. **Competing interests:** F.H., T.G., G.C., N.S., E.G., and F.S. are listed as inventors on corresponding pending patent applications in Italy (no. 102023000012279) and Portugal (no. 20232005054430) both filed on 15th June 2023 and titled "Quantum Bernoulli Factory photonic circuit independent of input state bias" dealing with schemes for the implementation of quantum-to-quantum Bernoulli factories. The authors declare that they have no other competing interests. **Data and materials availability:** All data needed to evaluate the conclusions in the paper are present in the paper and/or the Supplementary Materials.

Submitted 13 February 2024
Accepted 25 June 2024
Published 26 July 2024
10.1126/sciadv.ado6244